Open Access Journal

Journal of Power Technologies 95 (Polish Energy Mix) (2015) 14–22

journal homepage:papers.itc.pw.edu.pl

Experimental research and application possibilities of microcogeneration system with Stirling engine

Adrian Chmielewski*, Robert Gumiński, Stanisław Radkowski, Przemysław Szulim

Institute of Vehicles Faculty of Automotive and Construction Machinery Engineering
Warsaw University of Technology, 84 Narbutta Street, 02-524 Warsaw, Poland

Abstract

The first part of this paper presents the thermodynamic analysis for a microcogeneration system with the Stirling engine, for the most commonly used working gases, among others: helium, nitrogen, and air. The methods of regulating performance for the Stirling engine were depicted, among which the increase of gas pressure in the working chamber and rise in temperature of the upper heat source can be rated. The results of the experimental tests are shown: the influence of the rise in pressure and temperature on the working gases, which in this experiment were: helium, nitrogen, and air. The paper also focuses on maximum power flow. The tests were performed on a laboratory test stand with a single–action alpha type Stirling engine, located at the Faculty of Automotive and Construction Machinery Engineering, Warsaw University of Technology, at the Integrated Laboratory of the Mechatronic Systems of Vehicles and Construction Machinery. In the second part of the paper the authors presented the power flow in a hybrid system (Senkey diagram) on the internal combustion engine with the Stirling engine, which is employed as a microcogeneration device of distributed generation. It enables high-temperature waste heat to be transformed into mechanical work and transition of mechanical work into electric energy with the help of an electrical appliance, for possible sale to the mains. While analyzing the power flow in the hybrid cogeneration system, attention was paid to low-temperature heat which can be utilized through electrical thermogenerators, among other things. The proposed microgeneration assembly (Stirling engine and electrical thermogenerators) could be used to recover energy from waste heat produced by the combustion engine during combustion of landfill biogas. The influence of microcogeneration systems on boosting the general efficiency of the combustion engine was taken into consideration in this work. The paper presents test results of combustion gas temperatures in the exhaust system of the combustion engine fuelled by biogas, at full-load conditions. Various limitations of the Stirling engine build are discussed, in the context of cooperation with the combustion engine and the use of waste gases as a high-temperature heat source.

Keywords: Microcogeneration, Stirling engine, Thermodynamic analyses, Hybrid system

1. Introduction

Current requirements related to the efficiency of processing and utilization of primary energy (Directives 2009/28/EC [1] and 2012/27/EU [2]), as well as the prospect of limited fossil fuel resources point to an ever growing need to make use of cogeneration systems and to increase the share of renewable energy sources in the energy mix. There were *inter alia* combustion engines [3–5], steam engines [6], fuel cells [7, 8], microturbines [9], the Organic Rankine Cycle [10–12], Stirling engines [13–25], and many other items included among cogeneration technologies, described in detail in Directive 2012/27/EU. The abovementioned technologies open up options for achieving the EU target of a 20% increase in energy efficiency by 2020.

Growing attention is being paid to hybrid microcogeneration systems, for example: combination of the Stir-

*Corresponding author
Email address: a.chmielewski@mechatronika.net.pl (Adrian Chmielewski*)

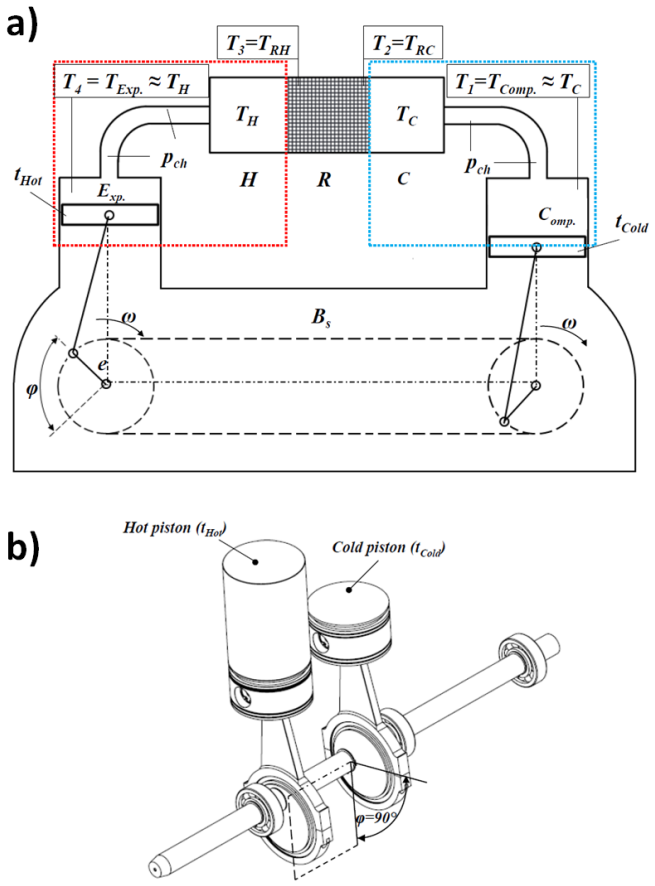

Figure 1: Demonstrative scheme of the Stirling alpha-type engine a), piston-crankshaft mechanism with angular travel marked φ=90° b)

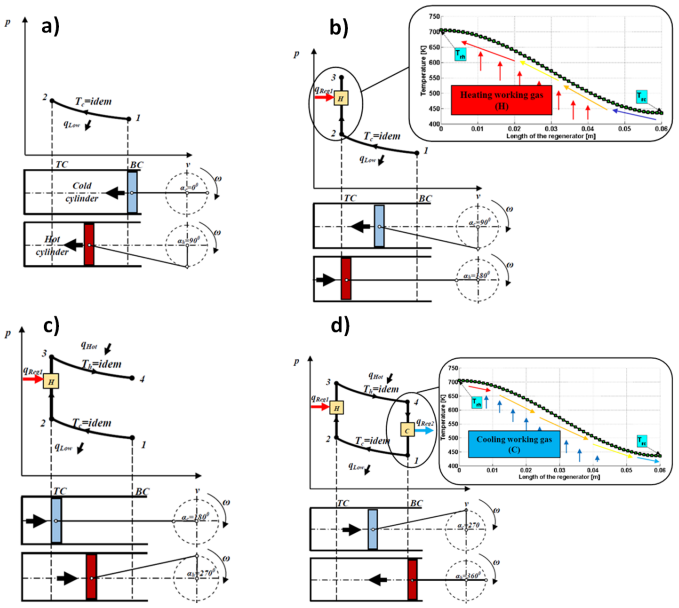

Figure 2: Accomplishment of the Stirling cycle for the engine in alpha configuration with angular travel φ=90° a) isothermal compression b) isochoric compression, c) isothermal expansion, d) isochoric expansion

ling engine and solar cells [21, 26, 27], the Stirling engine and fuel cells [8], and thermoelectric generators [28, 29], whose possible combination with the Stirling engine will be discussed in this paper. It is advisable to consider linking microcogeneration systems and renewable energy [26, 27, 30] sources to generate electricity for one's own purposes (prosumers [31]), and in bigger assemblies of distributed generation, limiting loss transfer for the target, final consumer.

2. Theoretical underpinnings and thermodynamic analysis

Thermodynamic analyzes are very important and in usual conditions they should precede experimental research [32–39]. Thermodynamic analyzes can take into account isothermal compression and expansion, adiabatic [32, 34, 36–39], or semi-adiabatic [40]. In the work herein the thermodynamic analysis was carried out in conditions where compression and expansion take place isothermally.

The theoretical Stirling cycle should be considered a cue when speculating analytically or with numerical calculations. Fig. 2a,b,c,d show the implementation of the theoretical Stirling engine cycle within the coordinates pressure-specific volume (p-v) for two pistons: the hot one t_{Hot}, which works in the expansion space E_{xp} and the cold one t_{Cold}, which works in the compression space C_{omp}. The Stirling cycle is accomplished by four thermodynamic transformations taking place one after another. During the cycle heat exchange takes place between the working gas, seen as ideal gas, and the environment. During isothermal process 1-2 at a constant temperature $T_{Comp.}$ that is equal to the temperature of the lower heat source (of cooler C with $T_c = idem$ Fig. 1a,b) and Fig. 2a) the heat q_{Low} is absorbed in the cooler at isothermal compression.The completion of the 1-2 transformation is marked by the reaching of the top stagnant position (TC) by piston T_{Exp}. During isochoric process 2-3 isochoric gas heating takes place—H point in Fig. 2b, the heat q_{Reg1} is delivered from the regenerator element (R—Fig. 1a)—the working gas is passed through the hotter regenerator (from T_{rc} to T_{rh}—the regenerator's element gives back the heat), which heats it. The working gas heated then in the heater acquires the temperature of the upper source T_h (the temperature gauged in the expansion space ($T_{Exp.}$—Fig. 1). During isothermal process 3-4 isothermal working gas expansion at temperature $T_h \approx T_{Exp.}$ takes place. During the isothermal expansion both the cold piston t_{Cold} working in the compression space $C_{omp.}$ (Fig. 2c) as well as the hot pis-

ton t_{Hot} working in the expansion space (E_{xp}) move in the same direction, allowing the working gas to expand. The heat q_{Hot} is delivered constantly by heater H to the working gas). This ensures that the gas is brought back to its original volume v_1 (at point 4 piston t_{Hot} reaches the lower stagnant position (BC)).

During isochoric process 4-1 (isochoric expansion)—passing back of the working gas (Fig. 2d) from the expansion space T_{Exp} can be observed. It takes place through (from the hot spot—heater T_{rh} to T_{rc}) the regenerator (the regenerator element has a lower temperature than the working gas—the regenerator absorbs the heat from the working gas—cooling working gas (C), the heat q_{Reg2} is taken from the working gas) up to the end of the regenerator element (where there is the temperature T_{rc}). The gas, after passing through the regenerator, is cooled down in the cooler to the temperature T_c (of the lower heat source), returns to point 1 and the whole heat cycle is completed.

It should be added that pressure p_{ch} (Fig. 1a) in the working space changes while the heat cycle is being accomplished. The pressure in buffer zone B_s (much bigger than the working chamber) is roughly constant during the heat cycle course. The piston stroke $e = 27.5$ mm (Fig. 1a), t_{Hot} and t_{Cold} piston diameter (Fig. 1b) equals $D = 110$ mm.

The Stirling heat cycle consists of four thermodynamic transformations. In processes 1-2 and 3-4 isothermal compression and expansion take place. The isothermal compression rate is $\varepsilon_{comp} = v_1 v_2^{-1}$, whereas the isothermal expansion rate is $\varepsilon_{exp} = v_3 v_4^{-1}$. For the Stirling cycle it is estimated that the isothermal compression rate equals the isothermal expansion rate $\varepsilon = \varepsilon_{comp} = \varepsilon_{exp} \Rightarrow v_1 v_2^{-1} = v_4 v_3^{-1}$. The detailed dependency describing the theoretical efficiency of the Stirling cycle including regeneration was described in paper [41] as:

$$\eta_{Stir_{reg}} = \frac{(\kappa - 1)(1 - \tau)\ln\varepsilon}{(\kappa - 1)\ln\varepsilon + \left(1 - \eta_{reg}\right)(1 - \tau)} \qquad (1)$$

Further to dependence (1), when the regenerator efficiency equals $\eta_{reg} = 1 \Rightarrow \eta_{Stir_{reg}} = 1 - \tau = \eta_{Carnot}$ the Stirling theoretical cycle efficiency is equal then to the thermal efficiency for the Carnot cycle (Fig. 3a,b, for the regenerator efficiency $reg_{eff} = 1$). In the case of there being no regeneration (lack of regenerator, Fig. 3—the regeneration efficiency equals zero $reg_{eff} = 0$) then:

$$\eta_{reg} = 0 \Rightarrow \eta_{Stir_{reg}} = \frac{(\kappa - 1)(1 - \tau)\ln\varepsilon}{(\kappa - 1)\ln\varepsilon + (1 - \tau)}$$

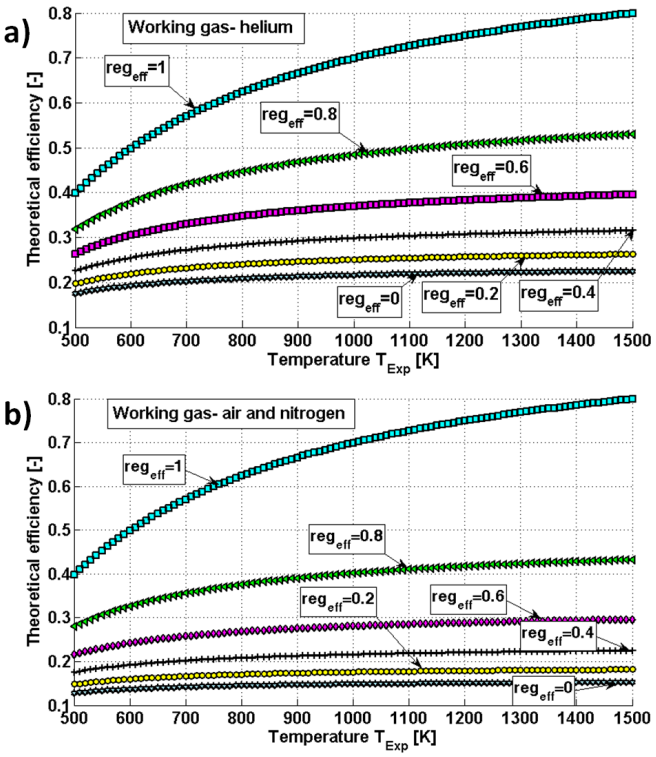

Figure 3: Influence of the regenerator's efficiency and upper heat source temperature on theoretical efficiency of the Stirling cycle, $\varepsilon = 1.6$, For nitrogen and air $\kappa = 1.4$. For helium $\kappa = 1.6$

Fig. 3 shows the influence of the temperature of the upper heat source and regenerator efficiency on the Stirling cycle at the preset compression rate and for the known temperatures of the lower $T_c = 301$ K and upper heat source $T_h = 901$ K for helium (Fig. 3a), nitrogen, and air (Fig. 3b).

The number of performed analyses indicate that with the increase in temperature of the upper heat source (with constant temperature of the lower heat source T_c), the theoretical efficiency of the Stirling cycle grows for all the considered working gases—helium, nitrogen, and air. Theoretical efficiency can be increased by applying the higher compression rate (Fig. 4) and the working gas, preferably monoatomic with a low molar mass and large isentropic exponent. The influence of the compression rate on the theoretical efficiency of the Stirling cycle is shown in Fig. 4. In practical engine use there are no edge ranges (0 and 1) of regenerator efficiency if the regenerator is used.

Analysis of Fig. 4 leads to the assumption that the highest efficiency increase by means of compression rate rise is achieved to $\varepsilon = 6$ for both: helium at the preset regenerator efficiency (reg_{eff}), and also nitrogen and air. The efficiency flows for nitrogen and air are practically the same (Figure 2b). This is due to the fact that both air and ni-

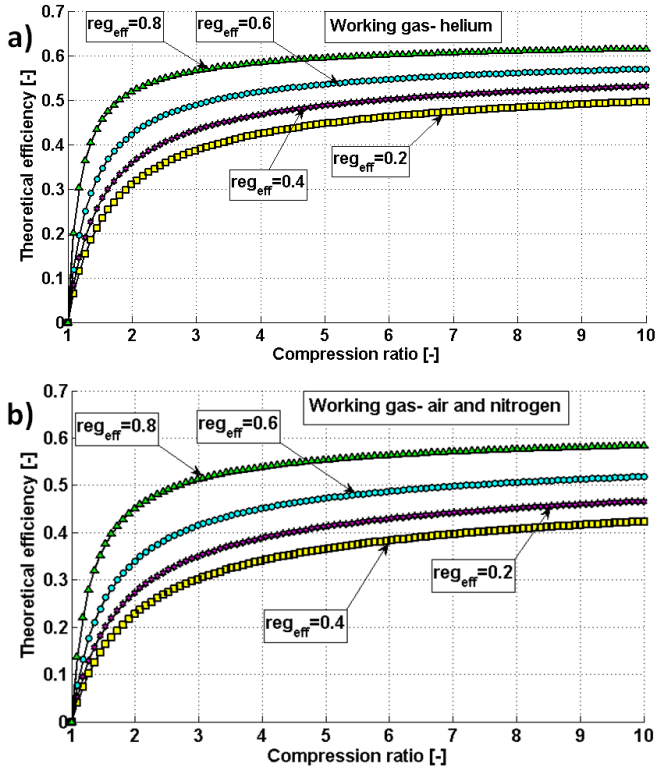

Figure 4: Influence of the regenerator's efficiency on theoretical efficiency of the Stirling cycle $\tau = 0.331$, $\varepsilon = 1.6$: a) for helium $\kappa = 1.66$, b) for nitrogen and air $\kappa = 1.4$

trogen are diatomic gases. In the case of treating air as a polyatomic gas (the air composition will include, for example, argon), the isentropic component will be $\kappa = 1.33$.

3. Description of the test stand—microcogeneration system with the Stirling engine

The test stand consisted of a one-action alpha type Stirling engine, a belt transmission of the gear ratio $i = 1 : 4$ between the Stirling engine and the direct current DC electric engine (nominal power of the electric engine 500 W), gauge sensors (the pressure transducer located in the cold cylinder, magneto-inductive sensor placed in the top stagnant position of the piston—synchronized with the notch on the gear wheel—TB), gauge thermocouples (K-type, located in: the compression space T_c, expansion space $T_{Exp.}$ and on the regenerator on the side of cooler T_{rc} and on the side of heater T_{rh}), the load-providing unit (the load-providing unit worked as the adjusted current source system of max. power 500 watts), National Instruments cards and the Labview software was used to register the chosen parameters. The working gas, helium, nitrogen and air in this case, was delivered from the cylinder (bottle) to buffer space p_b and working space p_c.

During the research the following factors were registered simultaneously: the temperatures in compression space T_{Comp}, in expansion space $T_{Exp.}$, on the regenerator on the cold T_{RC} and hot side T_{RH}, as well as the rotational speed on the Stirling engine (which was converted to the rotational speed on the electric engine at the known gear ratio between the electric engine and the Stirling engine $i = 1 : 4$), the current set by the load-providing unit, voltage on the electric engine and the pressure in the cold cylinder (compression space). The registration of every gauge point lasted 1 second. Adjusting the expense of the power delivered to the heater allowed for obtaining higher temperatures in the expansion space. In Fig. 5 pictures test stand a) and the outline of test stand b) are shown.

3.1. Experimental research results

The experimental research was carried out for helium, nitrogen and air. On the basis of the data obtained by means of measurements the speed characteristics were determined (Fig. 6) for different pressure values of the working gas at constant temperature in the expansion space. Blue lines in Fig. 7 mark the 11 bar pressure flow charts. The conducted research proves that the working gas mass delivered to the working chamber can change the average pressure of the working gas in the chamber, and as a result influence the performance of microcogeneration systems [38]:

$$P = L \cdot f = l \cdot \Updownarrow m_{gas} = l \cdot \frac{p_{gas} \cdot V_{gas}}{R \cdot T_{mean}} \cdot f \qquad (2)$$

On the basis of knowledge of input power P_{in} to the system, which was described in detail in [42], according to the dependence:

$$\eta_{\mu CHP} = \frac{P_{out}}{P_{in}} = \frac{P_{el}}{P_{in}} \qquad (3)$$

the efficiency of the microcogeneration system with the Stirling engine was determined. Fig. 7 depicts flows of maximum power shown as functions of the working gas pressure. Analysis of the depicted flows (Fig. 7a,b) indicates that according to the performed thermodynamic analysis, the highest performance values (the value of electric power) were obtained for helium—[42], which corresponds with 11.5% efficiency—Fig. 7b). For air 178.9 watts were obtained at 14 bars. It can be observed however, that within the range of pressure values 11...14 bars for air, the difference in maximum power values is slight, being only 3.5 watts. The efficiency for air at 14 bars was 5.2 %.
For nitrogen the maximum power was 159.5 watts at 11 bars, which corresponds with 4.7% efficiency. The maximum

power values were obtained for $T_{Exp.} = 910$ K and $T_{Comp.} = 301$ K.

In Fig. 8 the influence of the upper heat source (temperature measured in the expansion space $T_{Exp.}$) is shown for nitrogen. The tests were conducted for the temperature values 780 K, 850 K and 910 K. The temperature difference in the cooling circuit with changes of temperature of the upper heat source was negligible ($x < 10$ K). Analysis of Fig. 8 shows that an increase in the upper heat source significantly influences the values of the electric power obtained. The most evident improvement can be observed for pressure values up to 6 bars, where the electric power value between 780 K and 910 K is nearly twice as high. At 11 bars the blue line marks the electric power increase of almost 50 watts between the upper source of 780 K and 910 K.

4. Temperature measurements on the gas engine fueled with landfill biogas

Renewable energy sources and the possibility of obtaining certificates of highly efficient cogeneration undeniably raise interest on the side of owners of small biogas companies. In this part of the article the results of temperature measurements in the engine's exhaust system are presented. The engine was fuelled with landfill biogas [43]. The engine's nominal power is 1 MW, and the engine itself is pictured in Fig. 10. The value of waste heat high-temperature flow is approximately 0.5 MW, whereas the value of the flow of combustion gasses mass that pass through the exhaust system is $\dot{m} = 0.718$ kg/s.

Fig. 9 presents the flow charts of temperatures in the exhaust system in an engine fuelled with biogas. The tests performed proved that the exhaust gases temperature in the exhaust system does not exceed 500°C (1—in Fig. 9) at the full-load condition of the combustion engine with electric machinery at the speed of $n = 1500$ revs/min. The greater the distance from the engine, the lower the temperature on the outer walls (within 1.5 meters—it will be about 440°C).

For temperatures below 490°C use of the Stirling engine is problematic, but not impossible. The cues for designing the Stirling engine for microcogeneration purposes at lower temperatures are enumerated at 4.2 of this paper. A large number of steel elements displayed temperatures above 100°C (Fig. 10) which allows the use of passive cogeneration systems, including TEG (thermoelectric generators). Their structure and operation, as well as performance parameters, are discussed in the literature [28, 29].

4.1. Analysis of the load flow in a hybrid system for the combustion engine with microcogeneration systems

In the heat balance of the combustion engine a number of losses [43] occur. Among the most important are: exhaust losses of combustion gases (they have high temperatures), losses related to combustion engine cooling (the temperature of the coolant does not exceed 100°C), mechanical losses, piston friction in the cylinder sleeve, among others. From the point of view of energy conversion (heat – electric energy or mechanical energy) the losses in the exhaust system and in the cooling system are extremely important. Introducing cogeneration systems (Figure 11) with the external combustion Stirling engine (Zone 1—SE—the high-temperature section – exhaust system of the combustion engine) into the engine balance, in the exhaust system (Zone 2—TEG 2—low-temperature heat) and in the Stirling engine cooling system and the later section of the combustion engine exhaust system (medium- and low-temperature heat), we can submit a corrected formula for the absolute efficiency of the combustion engine:

$$\eta_{out\,all} = \eta_{ICE} + \eta_{cog1|SE} + \eta_{cog2|TEG2} + \eta_{cog3|TEG3} \quad (4)$$

or rendering it in a different form:

$$\eta_{out\,all} = \eta_{ICE} + \sum_{1}^{i=3} \eta_{cog} = \eta_{ICE} + \alpha_{cog\,all} \quad (5)$$

where: $\eta_{out\,all}$—absolute efficiency of the system comprising the combustion engine, cogeneration system with the Stirling engine, and cogeneration systems with thermoelectric generators, $\alpha_{cog\,all}$—indicator of the efficiency growth in comparison with the combustion engine without cogeneration systems.

Load flow in a microcogeneration system with the Stirling engine was analyzed in [42].

4.2. Cues for designing Stirling engines

Design of the Stirling engine requires most of all the defining of upper and lower heat source temperatures. Where the source of heat comes from exhaust gases (engine fueled with biogas), the active surface of heat exchange should be increased because their temperature in practice does not exceed 500°C. Moreover, the exhaust gases flow cannot be disturbed (the values of acceptable pressure drops in the exhaust system are usually mentioned in manufacturers' data catalogs of gas engines). What transpires from

the above is that the heater must be shaped in an appropriate and optimal way (heater pipes are usually placed parallel to the exhaust gases flow line) in order to most effectively absorb and exchange heat between the exhaust gases, the heater pipes, and the working gas in the external combustion engine. Depending on the optimal arrangement of pipes in the heater, construction options present themselves (one-action or two-action engine), and one engine or a set of engines take into account the decrease in exhaust gas temperature on the surface of the exhaust system. Also of great importance are: determining the efficiency of the heat exchangers, the diameter and the piston stroke in the crankshaft - piston system, the lubrication process and the choice of lubrication system (the non-lubrication system with a layer reducing friction or lubrication with the oil-mist [32, 37, 38]).

5. Summary/Conslusions

In the first part of this paper a thermodynamic analysis was conducted for the Stirling cycle. The influence of the upper source (T_{Exp}) temperature, compression degree, and the regenerator's heat efficiency on the theoretical efficiency of the Stirling cycle was determined. The analyses were carried out for the most frequently used working gases. The results of the analyses were confronted with the tests (the second part of the article), which allowed for an unambiguous statement that the temperature of the upper heat source influences the increase in the electric power value and general efficiency of the microcogeneration system with the Stirling engine. The experimental research performed also proved the legitimacy of applying helium (a monoatomic gas), for which efficiency levels were obtained that were more than twice those obtained with nitrogen or air.

Moreover, the possibility of applying the microcogeneration system with the Stirling engine on the gas engine fueled with landfill biogas was presented. The Senkey diagram shows a schematically pictured possibility of attaching the microcogeneration systems (the Stirling engine and thermoelectric generators) in order to increase the general efficiency of the combustion engine. The limitations connected with application of the Stirling engine were discussed.

References

[1] Directive 2009/28/EC of the European Parliament and of the Council of 23 April 2009, on the promotion of the use of energy from renewable sources and amending and subsequently repealing Directives 2001/77/EC and 2003/30EC.

[2] Directive 2012/27/EU of the European Parliament and of the Council of 25 October 2012 on energy efficiency, amending Directives 2009/125/EC and 2010/30/EU and repealing Directives 2004/8/EC and 2006/32/EC.

[3] F. Caresana, C. Brandoni, P. Feliciotti, C. M. Bartolini, Energy and economic analysis of an ice-based variable speed-operated micro-cogenerator, Applied Energy 88 (3) (2011) 659–671.

[4] G. Shu, Y. Liang, H. Wei, H. Tian, J. Zhao, L. Liu, A review of waste heat recovery on two-stroke ic engine aboard ships, Renewable and Sustainable Energy Reviews 19 (2013) 385–401.

[5] S. Wierzbicki, et al., Laboratory control and measurement system of a dual-fuel compression ignition combustion engine operating in a cogeneration system, Solid State Phenomena 210 (2014) 200–205.

[6] J. Fu, J. Liu, C. Ren, L. Wang, B. Deng, Z. Xu, An open steam power cycle used for ic engine exhaust gas energy recovery, Energy 44 (1) (2012) 544–554.

[7] A. Szczęśniak, J. Milewski, The reduced order model of a proton-conducting solid oxide fuel cell, Journal of Power Technologies 94 (2) (2014) 122–127.

[8] S. Obara, I. Tanno, S. Kito, A. Hoshi, S. Sasaki, Exergy analysis of the woody biomass stirling engine and pem-fc combined system with exhaust heat reforming, International Journal of Hydrogen Energy 33 (9) (2008) 2289–2299.

[9] M. Ismail, M. Moghavvemi, T. Mahlia, Current utilization of microturbines as a part of a hybrid system in distributed generation technology, Renewable and Sustainable Energy Reviews 21 (2013) 142–152.

[10] T. Wang, Y. Zhang, Z. Peng, G. Shu, A review of researches on thermal exhaust heat recovery with rankine cycle, Renewable and Sustainable Energy Reviews 15 (6) (2011) 2862–2871.

[11] I. Vaja, A. Gambarotta, Internal combustion engine (ice) bottoming with organic rankine cycles (orcs), Energy 35 (2) (2010) 1084–1093.

[12] J. Kalina, Integrated biomass gasification combined cycle distributed generation plant with reciprocating gas engine and orc, Applied Thermal Engineering 31 (14) (2011) 2829–2840.

[13] M. Renzi, C. Brandoni, Study and application of a regenerative stirling cogeneration device based on biomass combustion, Applied Thermal Engineering 67 (1) (2014) 341–351.

[14] D. García, M. González, J. Prieto, S. Herrero, S. López, I. Mesonero, C. Villasante, Characterization of the power and efficiency of stirling engine subsystems, Applied Energy 121 (2014) 51–63.

[15] G. Xiao, C. Chen, B. Shi, K. Cen, M. Ni, Experimental study on heat transfer of oscillating flow of a tubular stirling engine heater, International Journal of Heat and Mass Transfer 71 (2014) 1–7.

[16] E. Rogdakis, G. Antonakos, I. Koronaki, Thermodynamic analysis and experimental investigation of a solo v161 stirling cogeneration unit, Energy 45 (1) (2012) 503–511.

[17] H. Karabulut, H. S. Yücesu, C. Çınar, F. Aksoy, An experimental study on the development of a β-type stirling engine for low and moderate temperature heat sources, Applied Energy 86 (1) (2009) 68–73.

[18] C. Cinar, S. Yucesu, T. Topgul, M. Okur, Beta-type stirling engine operating at atmospheric pressure, Applied Energy 81 (4) (2005) 351–357.

[19] I. Batmaz, S. Üstün, Design and manufacturing of a v-type stirling engine with double heaters, Applied Energy 85 (11) (2008) 1041–1049.

[20] A. Sripakagorn, C. Srikam, Design and performance of a moderate temperature difference stirling engine, Renewable Energy

36 (6) (2011) 1728–1733.
[21] M. H. Ahmadi, H. Sayyaadi, S. Dehghani, H. Hosseinzade, Designing a solar powered stirling heat engine based on multiple criteria: maximized thermal efficiency and power, Energy Conversion and Management 75 (2013) 282–291.
[22] T. Li, D. Tang, Z. Li, J. Du, T. Zhou, Y. Jia, Development and test of a stirling engine driven by waste gases for the micro-chp system, Applied thermal engineering 33 (2012) 119–123.
[23] D. Thombare, S. Verma, Technological development in the stirling cycle engines, Renewable and Sustainable Energy Reviews 12 (1) (2008) 1–38.
[24] C.-H. Cheng, H.-S. Yang, L. Keong, Theoretical and experimental study of a 300-w beta-type stirling engine, Energy 59 (2013) 590–599.
[25] C. Cinar, H. Karabulut, Manufacturing and testing of a gamma type stirling engine, Renewable Energy 30 (1) (2005) 57–66.
[26] M. Abbas, B. Boumeddane, N. Said, A. Chikouche, Dish stirling technology: a 100 mw solar power plant using hydrogen for algeria, international journal of hydrogen energy 36 (7) (2011) 4305–4314.
[27] G. Chicco, P. Mancarella, Distributed multi-generation: a comprehensive view, Renewable and Sustainable Energy Reviews 13 (3) (2009) 535–551.
[28] K. T. Wojciechowski, J. Merkisz, P. Fuć, J. Tomankiewicz, R. Zybała, J. Leszczyński, P. Lijewski, P. Nieroda, Prototypical thermoelectric generator for waste heat conversion from combustion engines, Combustion Engines 52.
[29] K. Lubikowski, S. Radkowski, K. Szczurowski, M. Wikary, Analysis of possibility of use peltier modules in task of energy scavenging, Key Engineering Materials 588 (2014) 1–11.
[30] A. El Shahat, Pv module optimum operation modeling, Journal of Power technologies 94 (1) (2014) 50–66.
[31] A. Chmielewski, R. Gumiński, S. Radkowski, P. Szulim, Aspekty wsparcia i rozwoju mikrokogeneracji rozproszonej na terenie polski, Rynek Energii 114 (5) (2014) 94–101, in Polish.
[32] A. J. Organ, The regenerator and the Stirling engine, Wiley, 1997.
[33] M. Babaelahi, H. Sayyaadi, Simple-ii: A new numerical thermal model for predicting thermal performance of stirling engines, Energy 69 (2014) 873–890.
[34] R. Shoureshi, Analysis and design of stirling engines for waste-heat recovery, Ph.D. thesis, Massachusetts Institute of Technology (1984).
[35] T. Finkelstein, A. J. Organ, Air Engines, The American Society of Mechanical Engineers Press, New York, 2001.
[36] G. Walter, Stirling engines, Oxford University Press, Oxford, 1980.
[37] W. R. Martini, Stirling engine design manual, Martini Engineering, Washington (1983).
[38] S. Żmudzki, Stirling engines, PWN, Warsaw, 1993.
[39] D. Berchowitz, Stirling cycle engine design and optimalization, Ph.D. thesis, Ohio (1986).
[40] O. N. Igobo, P. A. Davies, Review of low-temperature vapour power cycle engines with quasi-isothermal expansion, Energy 70 (2014) 22–34.
[41] A. Chmielewski, et al., Thermodynamic analysis and experimental research on cogeneration system with stirling engine, Wulfenia Journal 21 (4).
[42] A. Chmielewski, S. Radkowski, S. Szczurowski, Analiza rozpływu mocy w układzie kogeneracyjnym z silnikiem stirlinga, Zeszyty Naukowe Instytutu Pojazdów 2 (2014) 98, in Polish.
[43] D. Gewald, K. Siokos, S. Karellas, H. Spliethoff, Waste heat recovery from a landfill gas-fired power plant, Renewable and Sustainable Energy Reviews 16 (4) (2012) 1779–1789.

Nomenclature

$\eta_{\mu CHP}$	microcogeneration system efficiency,
η_{ICE}	general efficiency of the combustion engine,
η_{reg}	regenerator's heat efficiency $(T_r\text{-}T_c)/(T_h\text{-}T_c)$, -
κ	isentropic exponent, $\kappa=c_p/c_v$
τ	temperature indicator (T_c/T_h), -
$\updownarrow m_{gas}$	working gas adjusted mass, kg
φ	angular travel, °
c_p	specific heat at constant pressure, J/(kg·K)
c_v	specific heat at constant volume, J/(kg·K)
D	piston diameter, mm
e	eccentricity, m
f	frequency, Hz
L	mechanical work, J
l	unit mechanical work, J/kg
P_{el}	electric power, W
p_{gas}	working gas medium pressure, Pa
P_{in}	input power, W
P_{out}	output power, W
$T_{Comp.}$	compression space temperature, K
$T_{Exp.}$	expansion space temperature, K
T_{mean}	working gas mean temperature, K
T_{rc}	temperature on the regenerator on the side of the cooler, K
T_{rh}	temperature on the regenerator on the side of the heater, K
T_r	temperature of the regenerator element $T_r=(T_h\text{-}T_c)/(\ln T_h/T_c)$, K
V_{gas}	working gas volume, m^3

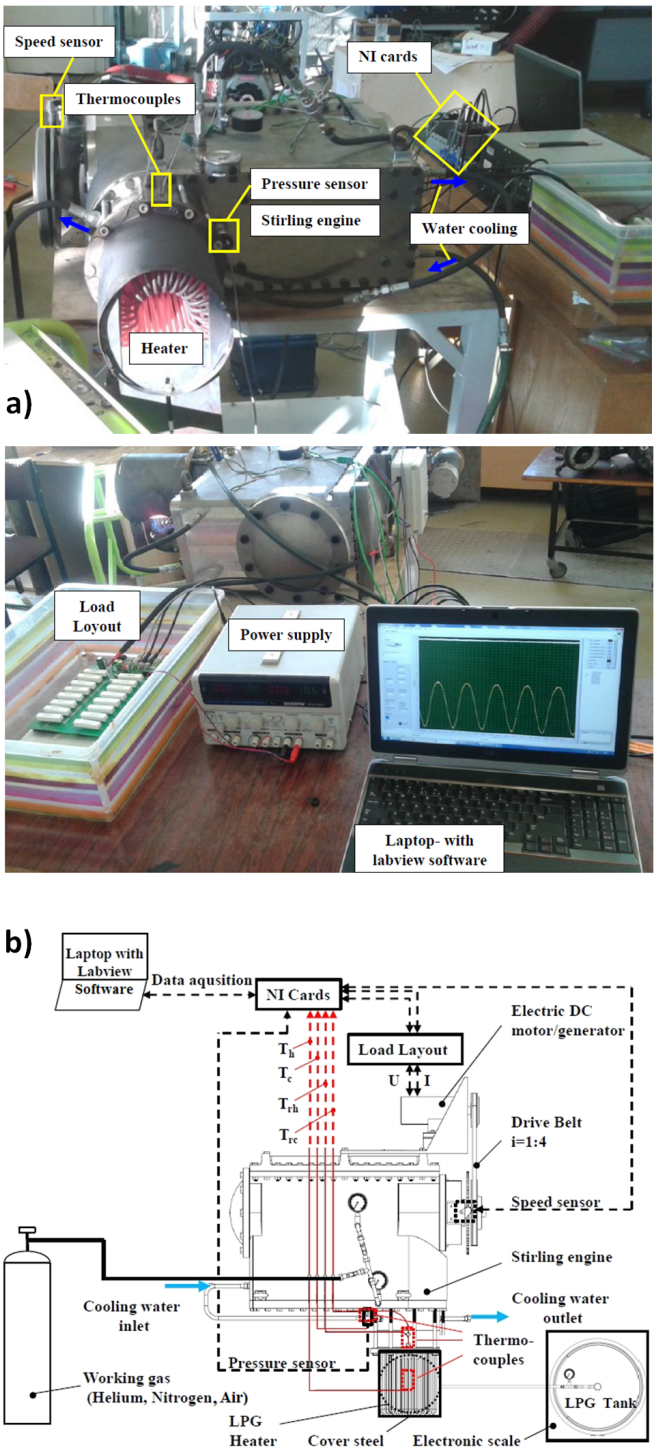

Figure 5: Pictures of the test stand a), demonstrative scheme of test stand b)

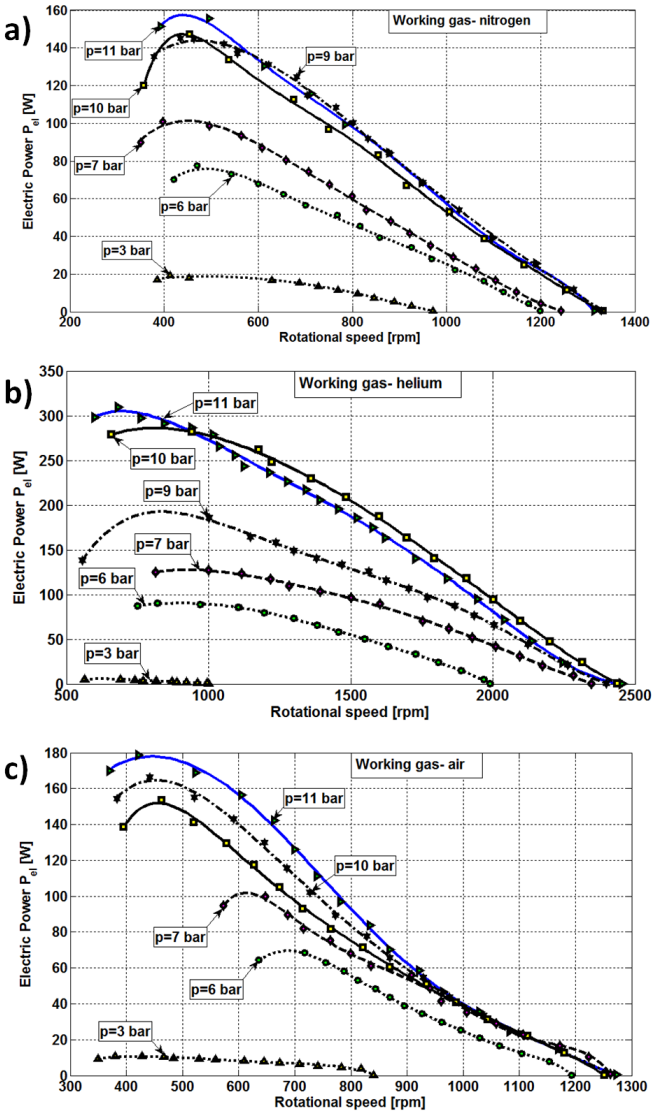

Figure 6: Speed characteristics a) nitrogen, b) helium, c) air

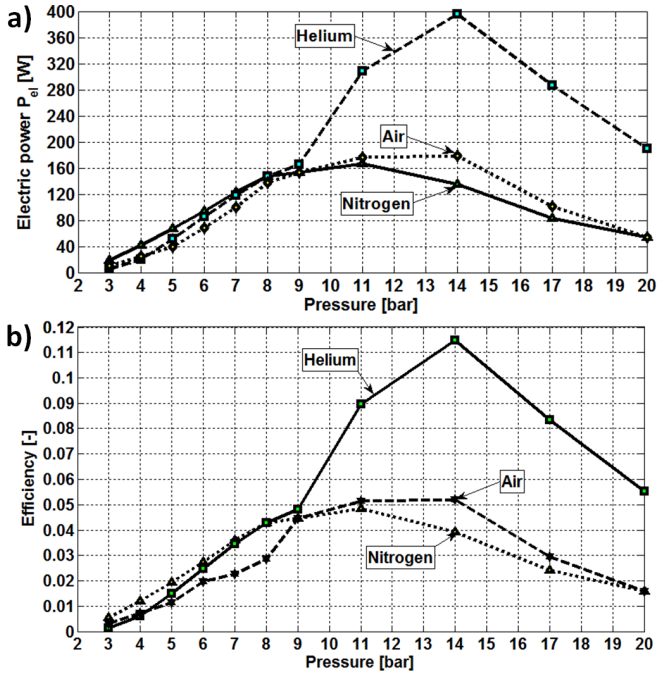

Figure 7: Max. power flowcharts a), for helium, nitrogen and air and efficiency b)

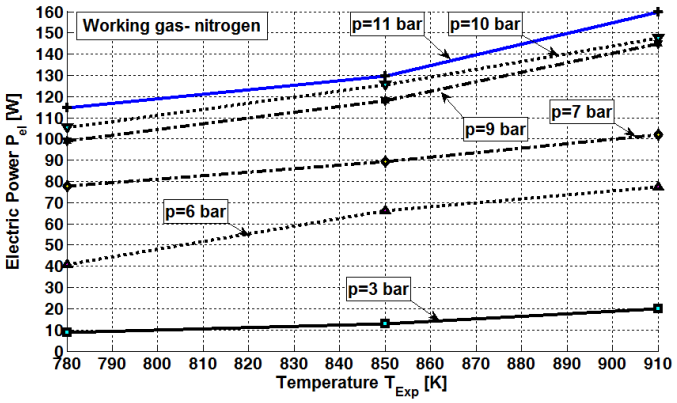

Figure 8: Flowcharts of influence of temperature in the expansion space on the electric power of the microcogeneration system—working gas nitrogen

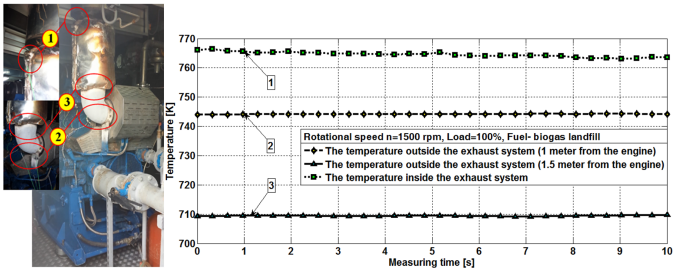

Figure 9: Flowcharts of temperature in the exhaust system in a combustion engine fuelled with landfill biogas

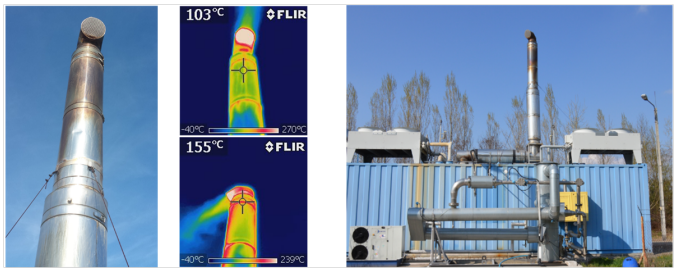

Figure 10: Visualization of the temperature flow obtained by infrared camera

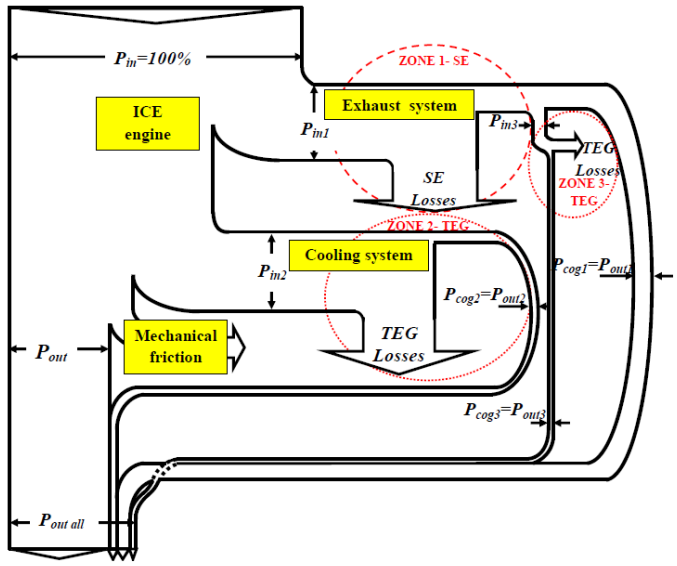

Figure 11: Sankey diagram for the combustion engine with cogeneration systems